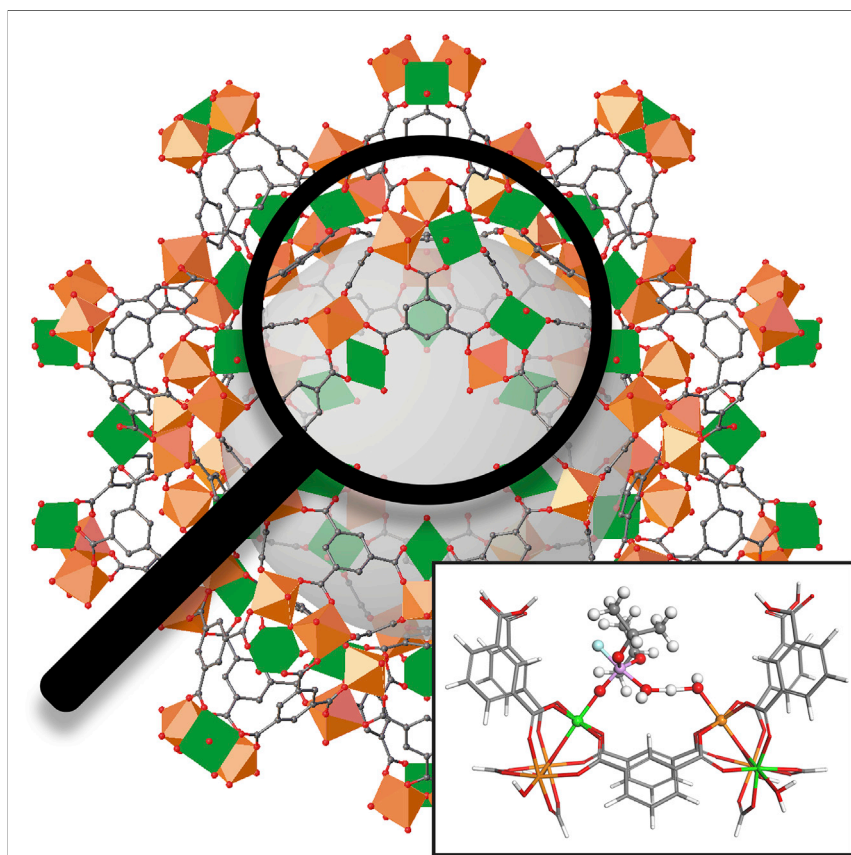# Chem

Article

Heterometallic Titanium-Organic Frameworks as Dual-Metal Catalysts for Synergistic Non-buffered Hydrolysis of Nerve Agent Simulants

A family of heterometallic titanium-organic frameworks is built from the combination of Ti(IV) with M(II) metal ions. Among them, only MUV-101(Fe) is capable of degrading the nerve agent simulant diisopropyl-fluorophosphate in non-buffered aqueous media, thanks to a dual-metal synergetic mechanism reminiscent of bimetallic enzymes. This work highlights the importance of controlling metal distribution in heterometallic frameworks at an atomic level for advancing the design of synergetic catalysts for unprecedented boosts in performance.

Javier Castells-Gil, Natalia -gnskip-->M. Padial, Neyvis Almora-Barrios, ..., Jorge A.R. Navarro, Sergio Tatay, Carlos Martí-Gastaldo

carlos.marti@uv.es

HIGHLIGHTS

Controlled distribution of metals in heterometallic titanium-organic frameworks

Dual-metal catalysis for degradation of chemical warfare agent simulants in water

Synergetic cooperation of Ti^{+4} and Fe^{+3} sites reminiscent of purple acid phosphatase

3 GOOD HEALTH AND WELL-BEING

9 INDUSTRY, INNOVATION AND INFRASTRUCTURE

Article

Heterometallic Titanium-Organic Frameworks as Dual-Metal Catalysts for Synergistic Non-buffered Hydrolysis of Nerve Agent Simulants

Javier Castells-Gil,[1,6] Natalia M. Padial,[1,6,7] Neyvis Almora-Barrios,[1,6] Rodrigo Gil-San-Millán,[2] María Romero-Ángel,[1] Virginia Torres,[2] Iván da Silva,[3] Bruno C.J. Vieira,[4] Joao C. Waerenborgh,[4] Jaciek Jagiello,[5] Jorge A.R. Navarro,[2] Sergio Tatay,[1] and Carlos Martí-Gastaldo[1,8,*]

SUMMARY

Mixed-metal or heterometallic metal-organic frameworks (MOFs) are gaining importance as a route to produce materials with increasing chemical and functional complexities. We report a family of heterometallic titanium frameworks, MUV-101(M), and use them to exemplify the advantages of controlling metal distribution across the framework in heterogeneous catalysis by exploring their activity toward the degradation of a nerve agent simulant of Sarin gas. MUV-101(Fe) is the only pristine MOF capable of catalytic degradation of diisopropyl-fluorophosphate (DIFP) in non-buffered aqueous media. This activity cannot be explained only by the association of two metals, but to their synergistic cooperation, to create a whole that is more efficient than the simple sum of its parts. Our simulations suggest a dual-metal mechanism reminiscent of bimetallic enzymes, where the combination of Ti(IV) Lewis acid and Fe(III)–OH Brönsted base sites leads to a lower energy barrier for more efficient degradation of DIFP in absence of a base.

INTRODUCTION

Metal-organic frameworks (MOFs) have emerged as a versatile platform to access a broad range of applications built upon their large structural and chemical diversity.[1] The unlimited number of combinations in which inorganic secondary building units (SBUs) can be linked to organic connectors by reticular design has been used to produce more than 84,000 porous crystalline frameworks[2] for promising advances in applications as gas storage and separation,[3,4] drug delivery,[5] or catalysis,[6,7] to cite a few. Among these, the degradation of chemical warfare agents (CWAs) and their simulants[8–10] has gained an increasing importance since early reports demonstrating the high activity of Zr-MOFs in the detoxification of nerve agents.[6,11,12] The activity of these materials originates from the presence of Zr_6 nodes that combine accessible Lewis acid Zr(IV) and basic-nucleophilic O^{2-}/OH^- sites, capable of activating P–X (X = F, O, S) bonds.

However, most detoxification studies have been carried out in the presence of basic buffers as N-ethylmorpholine, that behaves as a sacrificial base and a nucleophilic co-catalyst. In absence of this buffer, the catalyst is typically poisoned as result of the irreversible binding of the degradation products to the Zr(IV) active centers.[13] This problem can be partially overcome by heterogenization of basic-nucleophilic sites in the framework.[12,14–19] However, further improvement of CWA degradation remains limited by the intrinsic activity of the MOFs currently available.

The Bigger Picture

Heterometallic metal-organic frameworks (MOFs) can offer important advantages over their homometallic counterparts to enable targeted modification of their adsorption, structural response, electronic structure, or chemical reactivity. However, controlling metal distribution in these solids still remains a challenge. The family of mesoporous titanium-organic frameworks, MUV-101(M), displays heterometallic TiM_2 nodes assembled from direct reaction of Ti(IV) and M(II) salts. We use the degradation of nerve agent simulants to demonstrate that only $TiFe_2$ nodes are capable of catalytic degradation in non-buffered conditions. By using an integrative experimental-computational approach, we rationalize how the two metals influence each other, in this case, for a synergistic mechanism reminiscent of bimetallic enzymes. Our results highlight the importance of controlling metal distribution at an atomic level to span the interest of heterometallic MOFs to a broad scope of cascade or tandem reactions.
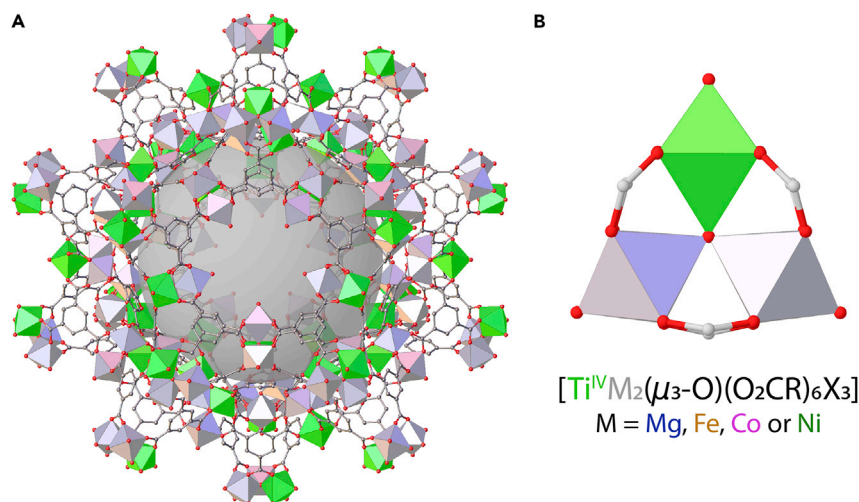
Figure 1. MUV-101 Heterometallic Titanium Organic Frameworks

(A and B) Structure of the family of mesoporous materials MUV-101 (A) assembled from the interlinking of heterometallic titanium clusters (B) with the formula [TiM$_2$(μ_3-O)(O$_2$CR)$_6$X$_3$] (M = Mg, Fe, Co, Ni; X = H$_2$O, OH$^-$, O^{2-}) and trimesate linkers.

In this regard, replacement of Zr(IV) with Ti(IV) might be beneficial due to its higher natural abundance, stronger Lewis acidity, and strength of Ti–O bonds.[20] Despite these promising features, the use of titanium-organic frameworks for the degradation of nerve agents has been only studied from a theoretical standpoint.[21] We argue that this lack of experimental information is due to the synthetic challenges intrinsic to the chemistry of titanium in solution. Compared with Zr(IV), this narrows the synthetic conditions required for targeting specific SBUs, thus restricting the assembly of targeted architectures.[22] We have recently reported the synthesis of MIL-100(Ti).[23] This mesoporous Ti-MOF is based on [Ti$^{IV}_3$(μ_3-O)(O$_2$CR)$_6$] metal-oxo clusters, also present in other frameworks based on trivalent metals as the archetypical MIL-100 family of Cr, Al, and Fe(III),[24] or other Ti(III) frameworks as COK-69[25] or MIL-101(Ti).[26] Previous works point out the versatility of the SBUs in accommodating different metals with variable charge for a persistent structure director.[27–31] We have demonstrated how the addition of a second metal for heterometallic titanium frameworks has proven an effective way to modify their photocatalytic activity by tuning of the band gap without compromising stability.[32] Following this strategy, the combination of Ti(IV) Lewis acid sites with other metal transition ions might result in synergetic cooperation for more efficient degradation of CWAs. Just like purple acid phosphatase (PAP) metalloenzymes that combine Fe^{3+} and M^{2+} in the active centers,[33] heterometallic Ti-MOFs might also enable dual-metal catalysis for superior activity compared with homometallic Zr(IV) analogs.

We demonstrate this concept for a new family of heterometallic titanium MUV-101(M) frameworks (M = Mg, Fe, Co, and Ni) isostructural to the archetypal MIL-100 family (Figure 1).[24] These mesoporous materials can be prepared from direct reaction of the molecular precursors to ensure good control over the distribution of the metals across the structure. Compared to post-synthetic doping of preformed materials, that can result in partial or non-homogeneous metal substitution,[34] we argue that homogeneity is fundamental to rationalize the effect of the heteroatom over activity. Our results show that pristine MUV-101(Fe) displays excellent catalytic activity for the degradation of the Sarin gas simulant DIFP (diisopropyl fluorophosphate) in water and non-buffered conditions. This distinctive behavior, that is not accessible

[1]Functional Inorganic Materials Team, Instituto de Ciencia Molecular (ICMol), Universitat de València, Paterna 46980, València, Spain

[2]Departamento de Química Inorgánica, Universidad de Granada, Avenida Fuentenueva S/N, Granada 18071, Spain

[3]ISIS Facility, Rutherford Appleton Laboratory, Chilton, Didcot, Oxfordshire OX11 0QX, UK

[4]Centro de Ciências e Tecnologias Nucleares, Instituto Superior Técnico, Universidade de Lisboa, Bobadela LRS 2695-066, Portugal

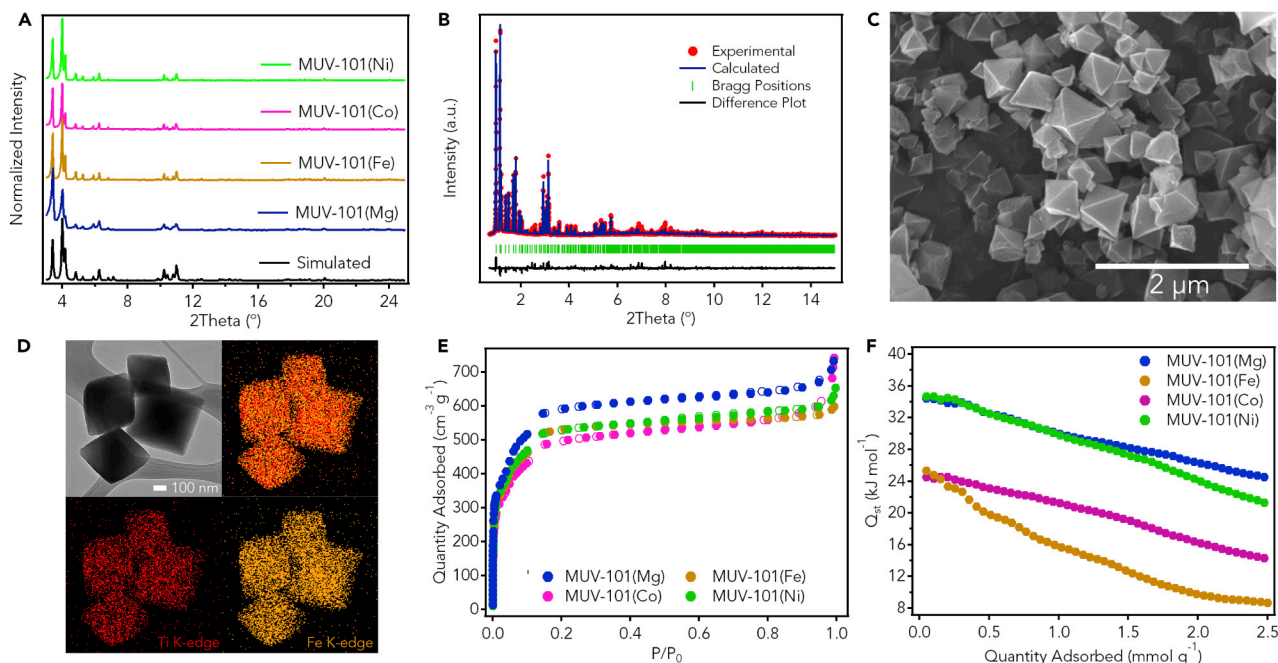[5]Micromeritics Instrument Corporation, 4356 Communications Drive, Norcross, GA, USA

[6]These authors contributed equally

[7]Present address: Department of Chemistry, Scripps Research, 10550 North Torrey Pines Road, La Jolla, CA 92037, USA

[8]Lead Contact

*Correspondence: carlos.marti@uv.es

https://doi.org/10.1016/j.chempr.2020.09.002

Figure 2. Characterization of MUV-101 Heterometallic Titanium-Organic Frameworks
(A) Comparison of the PXRD of MUV-101(Mg, Fe, Co and Ni) solids with the pattern simulated from the structure refined for MUV-101(Fe).
(B–D) Rietveld refinement of MUV-101(Fe) ($\lambda = 0.442655$ Å) (B), SEM micrograph (Scale bar: 2 µm) (C), and TEM-EDX mapping images of as-synthesized MUV-101(Fe) crystals (D) (scale bar: 100 nm).
(E) N_2 adsorption-desorption isotherms of MUV-101 solids at 77 K.
(F) Calculated isosteric heat of adsorption of CO_2.

to its homometallic counterparts or other heterometallic combinations, results from the synergetic cooperation of Ti(IV) and Fe(III) sites in close proximity for a cooperative mechanism that mimics bimetallic phosphatases.

RESULTS AND DISCUSSION

Heterometallic MUV-101 Titanium-Organic Frameworks

MUV-101 heterometallic [TiM$_2$(μ_3-O)(L)$_2$X$_3$] (M = Mg, Fe, Co, Ni; L = benzene-1,3,5-tricarboxylate; X = H$_2$O, OH$^-$, O^{2-}) materials were synthesized by using similar conditions to those reported for the heterometallic titanium-framework MUV-10.[32] In a typical experiment, titanium(IV) isopropoxide was reacted with benzene-1,3,5-tricarboxylic acid and the corresponding chloride metal salts, in a mixture of *N,N*-dimethylformamide (DMF) and acetic acid (AcOH) at 120°C (See Section S2 for experimental details). After 48 h, the resulting microcrystalline materials were separated by centrifugation, washed with copious amounts of DMF and methanol (MeOH), and allowed to dry under reduced pressure. Compared with our previous method based on metal exchange reactions with MUV-10,[35] this one-step synthesis can be easily scaled-up to larger volume vessels to produce close to 1 g of material per reaction batch. Also, the use of higher temperatures enables the formation of pure MUV-101(Fe) phases not accessible at 65°C.

Phase purity of the solids was confirmed with powder X-ray diffraction (PXRD), thermogravimetric analysis (TGA), scanning electron microscopy (SEM), and inductively coupled plasma mass spectrometry (ICP-MS). LeBail refinement of the PXRDs converged in a cubic *Fd-3m* space group with excellent residual values in all cases to confirm the formation of pure crystallographic phases isostructural to MIL-100

(Figures 2A, S1, and S2; Table S3).[24] Rietveld refinement was performed on MUV-101(Fe) as a representative example of this family of heterometallic solids (Figure 2B; Table S2). TGA ruled out the formation of contaminant oxide phases, based on the good agreement between the experimental and calculated weight percentages of residue that results from thermal decomposition of the solids in air. Compared with the homometallic MIL-100(Ti),[23] the substitution of Ti(IV) with softer M(II) metals reduces the temperature at which the heterometallic phases decompose in synthetic air, from 450°C down to a minimum of 350°C (Figure S4; Table S4). As for the microscopic structure, SEM revealed all solids to be composed of submicrometric particles with octahedral morphologies and a homogeneous size dispersion of ca. 1 μm (Figures 2C, S5, and S6). Energy dispersive X-ray spectroscopy (EDX) single-point mapping measurements reveal average ratios close to 1:2 (Ti:M), consistent with the formation of heterometallic $[TiM_2(\mu_3-O)(O_2CR)_6X_3]$ clusters. Agreement with the proposed formula was also corroborated with ICP analysis (Table S1). The homogeneous distribution of both metals throughout the solid was used to discard metal clustering (Figures 2D and S7–S11). To confirm the formation of heterometallic solids rather than segregated homometallic phases, we also ran control experiments by individual reaction of the linker, with each metal precursor under the same conditions used for the synthesis of MUV-101. Whereas reactions with Mg, Co, or Fe(II) led to clear solutions and no solid could be isolated, reaction with Ti(IV) or Ni(II) produced an amorphous solid or a different crystalline phase, respectively (Figure S3). These experiments suggest that the simultaneous presence of Ti(IV) and M(II) metals in the reaction medium is necessary to induce the assembly of the heterometallic TiM_2 metal-oxo clusters required for the formation of the framework. The heterometallic nature of the local structure of the cluster was confirmed with synchrotron X-ray total scattering and pair distribution function (PDF) analysis of MIL-100(Fe), MIL-100(Ti), and MUV-101(Fe). Compared to the homometallic frameworks that display a single peak in the M–M region, MUV-101(Fe) shows the presence of two contributions to that intermetallic region (Figure S12). Further analysis of the M–O, M–C, and M–M contributions from the differential PDFs confirms that the M–M distances in heterometallic MUV-101(Fe) are clearly different from those displayed by homometallic MIL-100 phases (Figure S13; Table S5). These changes are consistent with the incorporation of Ti and Fe into a heterometallic $TiFe_2$ metal-oxo cluster, ruling out the coexistence of segregated homometallic phases or clusters that would simply correspond to the superposition of the signals corresponding to the individual Ti–Ti and Fe–Fe homometallic components. Nonetheless, we note that further techniques, as neutron powder diffraction and neutron total scattering experiments might be necessary to unambiguously assess the metallic distribution along the seven crystallographically independent metal sites in MUV-101(M) materials.

Permanent porosity of the MUV-101(M) family was analyzed with N_2 isotherms at 77 K (Figure 2E). All solids show a reversible type-I isotherm with no hysteresis and two additional uptakes at P/P_0 = 0.04 and 0.12, due to the filling of the two type of mesopores characteristic of the mesoporous structure of MIL-100. The experimental Brunauer-Emmet-Teller (BET) surface areas for all solids oscillate between 1,840 and 2,200 $m^2 \cdot g^{-1}$ (Figures 2E and S14–S17). These values are in good agreement with those described for other MIL-100 phases[36] and exceed the 1,320 $m^2 \cdot g^{-1}$ reported for homometallic MIL-100(Ti). The pore size distribution (PSD) was calculated by non-linear density functional theory (NLDFT) methods and reveals two types of mesopores of ca. 17–21 and 22–26 Å, consistent with the crystallographic structure refined for MUV-101(Fe). CO_2 adsorption isotherms collected between 273 and 293 K show clear differences in the adsorption profile that can be attributed to the

incorporation of different divalent metals to the framework (Figures S18A–S18D). Changes are likely due to the different interaction of CO_2 molecules with the vacant M sites generated during the activation of the solids by thermal heating in vacuum. The isosteric heats of adsorption vary according to the sequence Mg ≈ Ni > Co > Fe (Figure 2F). Similar trends have been observed for MOF-74 upon replacement of Mg with Ni or Co(II), highlighting the impact that metal substitution can have on tuning the selectivity of gas adsorption.[37] We also estimated the impact of incorporating Ti(IV) sites on the number of open metal sites accessible by thermal activation, by using water adsorption isotherms according to a recently reported protocol (Figures S19 and S20; Table S7).[38] Compared to homometallic MIL-100 materials, MUV-101(Fe) displays a smaller number of open metal sites per formula unit (1.68). This agrees well with the proposed formula as the excess of charge that results from the incorporation of highly charged Ti(IV) units to the cluster must be counterbalanced by negatively charged species (OH$^-$, O^{2-}); thus reducing the number of water molecules per cluster available.

One of the main limitations of MOFs for broad range application is their limited chemical stability, in particular to water. This might be an issue for the degradation of nerve agents, as these experiments generally require buffered aqueous solutions or the formation of acid molecules as the reaction product. Accordingly, we evaluated the hydrolytic stability of MUV-101 solids under acid and basic conditions (See Section S5 for details). Except for MUV-101(Mg), which showed very poor stability leading to complete degradation of the solid even in pure water (Figure S21), the PXRD profiles of the rest of materials remained intact after soaking during 24 h in water solutions at pH between 2 and 12 (Figures S22–S24). At first, this suggested a good hydrolytical stability, but we also collected N_2 isotherms of the solids after the treatment to confirm this point. From a porosity standpoint, only MUV-101(Fe) retains the original properties and can be considered stable toward the attack of water. MUV-101(Ni) and MUV-101(Co) suffer from a partial loss in the BET value that reaches a maximum of close to 60% for the heterometallic Ni(II) phase in basic conditions (Figures S25–S27; Tables S9–S11). These changes in hydrolytical stability linked to M(II) replacement were further confirmed by ICP and SEM analysis (Figures S28–S31; Table S12). This shows a higher concentration of M(II) in solution for MUV-101(Co, Ni), also associated with a reduction in particle size and morphology, which could compromise the long-term stability of these materials in water given the presence of labile M(II)–O bonds. We argued the higher stability of MUV-101(Fe) was probably due to the presence of stronger Fe(III)–O coordination bonds, less likely to undergo water hydrolysis. This was confirmed with Mössbauer spectroscopy measurements of MUV-101(Fe) (Figure 3; Table S8), which revealed the complete transformation of Fe(II) into Fe(III) in the final material. It is worth noting that all our attempts to synthesize heterometallic MUV-101(Fe) from Fe(III) salts under analogous reaction conditions were unsuccessful. This suggests the inability of heterometallic TiM$_2$ SBUs to incorporate metals with higher oxidation states directly from solution. Just like for the case of Fe-MOF-74, the gradual oxidation of Fe(II) sites after incorporation to the framework is possibly more respectful with the structure formed originally.[39]

Catalytic Activity for the Detoxification of Chemical Warfare Simulants in Non-buffered Conditions

Phosphonate-based nerve agents can act as inhibitors of the acetylcholinesterase enzyme (AChE), present in the central nervous system, by causing a continuous stimulation of the nerve fiber for asphyxiation and death. This family of molecules
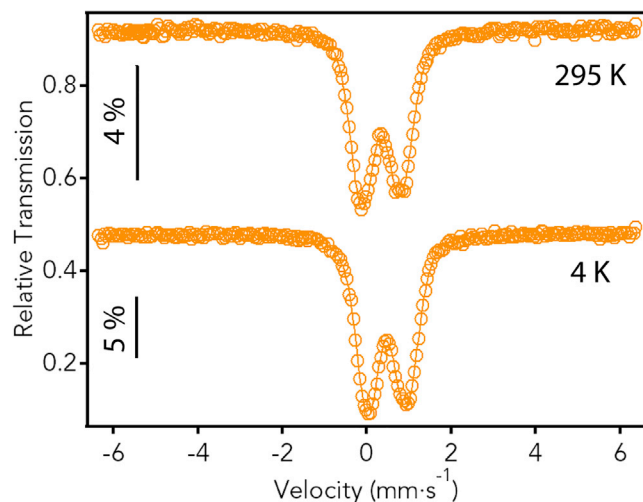
Figure 3. Mössbauer Spectra of MUV-101(Fe) at 295 and 4 K Confirm the Presence of Fe(III) in the Framework

generally display a stereogenic P(V) center with one P=O bond and one alkyl (–R), one fluoride (–F) and/or –XR residues (X= O, S, N). Their degradation involves the hydrolysis of P–F or P–XR bonds to form non-toxic phosphate or alkylphosphonic acids (Figure 4A).[40] Some metalloenzymes, such as phosphotriesterases, are capable of hydrolyzing phosphate ester bonds through cooperative catalysis between the two metals that form the active site. We hypothesized that the combination of a Ti(IV) Lewis acid site with another metal ion in the heterometallic [TiM$_2$(μ_3-O)(O$_2$C)$_6$X$_3$] cluster of MUV-101 might mimic the activity of the metalloenzyme PAP that displays bimetallic Fe(III)–M(II) active sites. To prove our hypothesis, we tested the activity of the MUV-101 family for the degradation of DIFP, a simulant of the Sarin nerve agent. Initial experiments were carried out in non-buffered aqueous solutions with an equimolar MOF:DIFP ratio (See Section S6 for experimental details). Figures 4B and 4C shows the hydrolysis reaction profiles of MOF:DIFP 1:1 mixtures in the presence of heterometallic MUV-101 materials, homometallic MIL-100(Ti), MIL-100(Fe) and their physical mixture in a 1:2 ratio respectful with the composition of the heterometallic cluster in MUV-101(Fe). Noteworthy, MUV-101(Fe) is the only one that degrades 100% of the agent within 490 min in non-buffered aqueous solution at room temperature with a half-life time of 165 min for the formation of diisopropylphosphate (DIP) as detected by ^{1}H and ^{31}P-NMR (Figures S40–S43). The half-life time can be reduced to 8 min when using an excess of catalyst (Figures S32 and S33; Table S14). It is worth noting that MUV-101(Fe) shows a multi-step degradation profile that combines a rapid increase up to 25 min, associated to the uptake of DIFP by the substrate, followed by a sigmoidal profile reminiscent of allosteric enzymes. This shape suggests a cooperative process, that in our case, might correspond to the fixation of the substrate at Lewis acid Ti(IV) sites followed by its degradation supported by Fe(III)–OH Brönsted basic sites. This is consistent with the analysis of the reaction mixture during the catalytic tests, which confirms that degradation is negligible until 100 min (Figure S35). Control experiments, ran in absence of MUV-101(Fe), also confirm the inability of DIFP to degrade in the same experimental conditions after 48 h. The catalytic nature of DIFP detoxification with MUV-101(Fe) was demonstrated by varying the MOF:DIFP ratio from 1:1 to 1:10. DIFP is fully degraded in all cases but the rate of transformation slows down with the concentration of the substrate down to a maximum half-life of 802 min for 1:10 ratio (Figure 4D). The heterogeneous nature
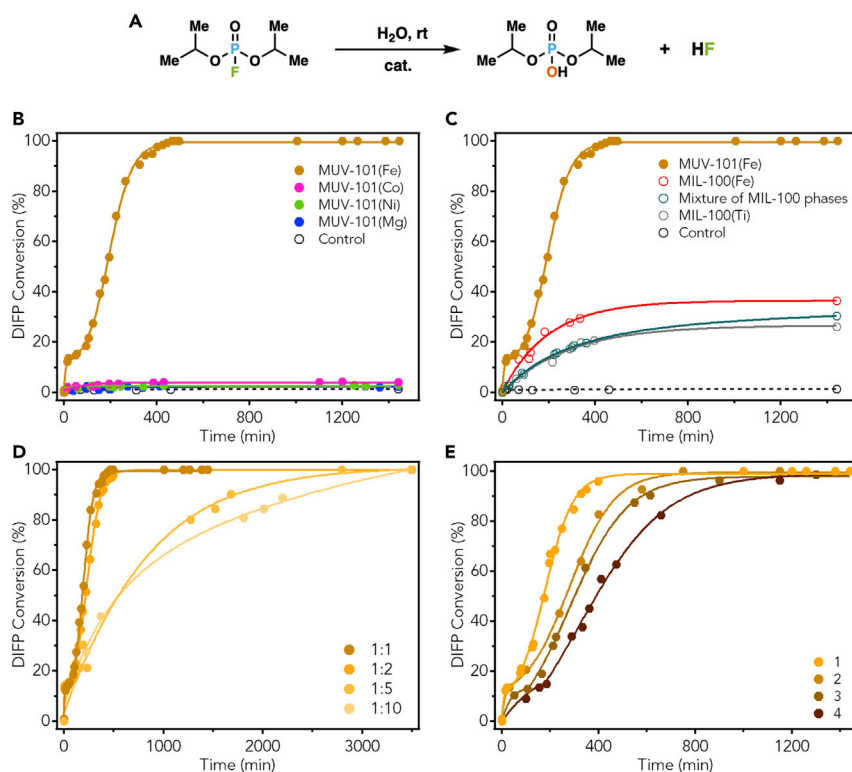
Figure 4. Detoxification of Nerve Agents with Heterometallic MUV-101 Frameworks

(A) Scheme of the hydrolytic degradation of DIFP.

(B) Hydrolysis profiles of DIFP of MUV-101(Mg, Fe, Co, and Ni) the family in water.

(C) Comparison of the activity of MUV-101(Fe) with homometallic MIL-100(Ti and Fe) and their physical mixture.

(D) Variation of the reaction kinetics with the MUV-101(Fe):DIFP ratio.

(E) Cyclability of MUV-101(Fe) for four consecutive catalytic tests for a fixed 1:1 ratio.

of the catalytic process was also confirmed by filtrating the catalyst after 2 h, which resulted in an immediate drop of activity (Figure S36).

Compared to MUV-101(Fe), MIL-100(Ti), MIL-100(Fe), MUV-101(Mg, Co, Ni), MUV-10(Mn),[32] and UiO-66(Zr),[41] all display a poor performance or become poisoned by DIFP degradation products[13] in non-buffered aqueous catalytic conditions (Figures S37 and S38). To find out if the poor activity of the other titanium homometallic and heterometallic frameworks might be due to their partial degradation in the reaction conditions, we examined their stability after 24 h by using PXRD. Our results confirmed the stability trends in water. MUV-101(Mg) is not stable in the reaction conditions but the rest of the solids did not show any sign of structural degradation and remained highly crystalline after the catalytic tests (Figure S50), suggesting that the poorer activity of MUV-101(Co, Ni) must have a different origin. Extraction of the reaction mixture with dichloromethane after 24 h of reaction shows no presence of unreacted DIFP in the case of MUV-101(Fe), whereas for homometallic MIL-100(Ti), MIL-100(Fe) and their physical mixture allowed to recover close to 100%, 91.7%, and 97.3% of the nerve agent added at the beginning of the tests (Figure S37B). This suggests that adsorption of the guest DIFP and not degradation dominates the changes in DIFP concentration over time in the homometallic MIL-100 solids. To put our results in a more general context, we have also compared our results with the performance reported for the most representative MOFs used

in the degradation of CWAs or their simulants in different experimental conditions (Tables S15 and S16). MUV-101(Fe) is the only pristine MOF capable of catalytic degradation of DIFP with no signs of catalyst poisoning in non-buffered aqueous media without the presence of a basic-nucleophilic co-catalyst (i.e., *N*-ethylmorpholine, dimethylaminoepyridine, or metal-alkoxide). This is a remarkable result in comparison with the state-of-the-art Zr-MOF materials currently in use.[19] To confirm this point, we tested MUV-101(Fe) and UiO-66 under equivalent conditions to identify the product of the reaction and quantify the poisoning of the catalyst. Analysis of the ^{1}H NMR and ^{31}P-NMR spectra of the supernatant and the solids after digestion in NaOD/D$_2$O (2M) confirms that the product of the reaction is exclusively DIP in both cases. Compared to UiO-66 that adsorbs close to 25% of DIP, the poisoning of MUV-101(Fe) is minor and drops down to 5% (See Section S6). Also important, MUV-101(Fe) can endure three consecutive reuses without substantial reduction of its catalytic activity (Figure 4E). Similar activities have been reported for UiO-66-0.25NH$_2$@LiO^{t}Bu[16] and NU-1,000@Mg(OMe)$_2$_1:4[19], but these materials require a pre-treatment with strong basic agents and suffer from poorer cyclability.

Overall, our findings suggest that the catalytic activity of pristine MUV-101(Fe) cannot be explained by the association of these two metals but to their synergistic cooperation to create a whole that is more efficient than the simple sum of its parts. Like bimetallic PAP enzymes and other biological systems, this heterometallic titanium framework seems to display the activity expected for a dual-metal catalyst, in which the two different metals, Ti(IV) and Fe(III), act simultaneously on two different substrates, DIFP and water, to accelerate the hydrolysis reaction.

Dual-Metal Synergistic Degradation Mechanism in MUV-101(Fe)

To guide this study, we used the mechanism proposed in the literature for bimetallic PAP as a reference.[33,42] The active center of these enzymes is based on binuclear (HO)–Fe^{III}–(μ-OH)–M^{II}–(H$_2$O) units. Hydrolysis of phosphate esters in PAP undergoes by activation of the P=O at M(II) acting as a Lewis acid site, whereas the neighboring Fe(III) –OH centers act as a Brönsted base, activating the hydrolysis of water to generate nucleophilic OH-anions that will ultimately attack the P(V) atom. We used computational modeling to rationalize our experimental results on the basis of this mechanism to understand why MUV-101(Fe) outperforms other isostructural homo- and heterometallic systems in the degradation of DIFP (See Section S7 for details).

As depicted in Figure 5A, this would involve the activation of DIFP and water at neighboring metal sites in the framework. The steric hindrance and lack of accessible coordination sites revealed that hydrolysis was not possible for one single cluster, thus pointing to a cooperative mechanism (Figure S51). Hence, we modeled the interaction of the DIFP molecules between two adjacent SBUs in the mesoporous cage of MUV-101(Fe). By using density functional theory (DFT), we first investigated the activation of DIFP by water displacement at the metal axial positions in heterometallic MUV-101(Fe, Co) and homometallic MIL-100(Fe, Ti) (Figure 5B, stage 0). For simplicity, we used MUV-101(Co) as representative of the poor performance of the MUV-101(Mg, Ni, Co) phases. In a first step, DIFP molecules were allowed to interact directly with the metal atom upon release of the axially coordinated water molecule (Figure 5B, stages 0–2). This competitive stage is exothermic in all cases and results in DIFP binding to the axial position of Ti(IV) through the P=O group, with adsorption energies (E$_{ads}$) ranging from −53.1 for MIL-100(Ti) to −33.8 kJ mol^{-1} for MUV-101(Co) (Figures 6 and S52; Table S17). In all cases,
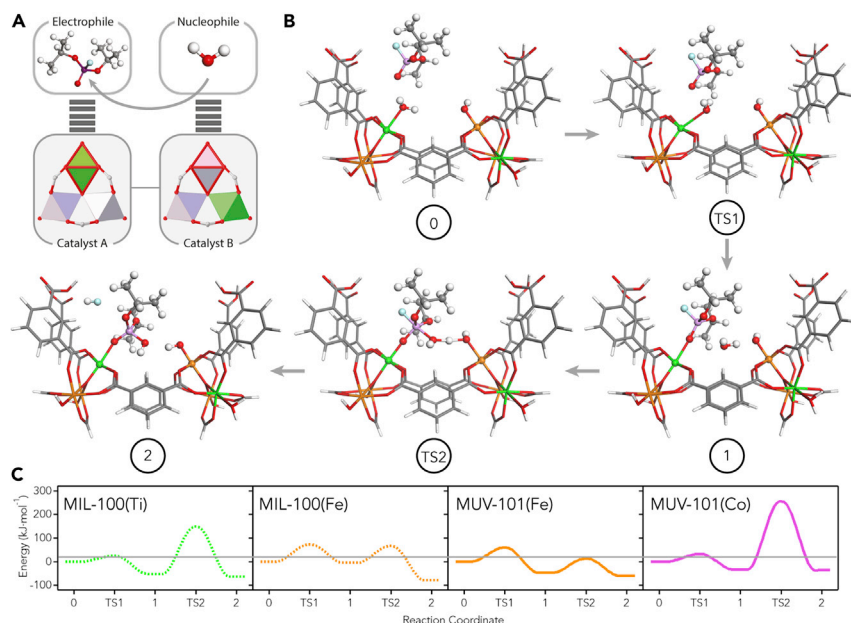
Figure 5. Proposed Mechanism for Dual-Metal Catalytic Detoxification in Heterometallic MUV-101(Fe)

(A) Scheme illustrating the cooperative activation of DIFP and water at neighboring metal sites in the framework.

(B) Proposed reaction mechanism for the dual-metal synergetic degradation of DIFP with MUV-101(Fe) involving Ti(IV) (green) and Fe(III) (orange) sites. Step 0: Initial state of reactants and catalyst. Transition State 1(TS1): Transition state of water displacement by DIFP molecules. Step 1: Adsorption of DIFP on the active site of Ti(IV) ions. Transition State 2 (TS2): Transition state of the nucleophilic attack on the P(V) center by activated water molecules. Step 2: Release of HF.

(C) Reaction energy profile for homometallic MIL-100(Ti and Fe) (dashed lines) and heterometallic MUV-101(Fe and Co) (solid lines).

coordination of DIFP in Ti(IV) metal sites is clearly preferred over Co(II) or Fe(III), likely due to the stronger Lewis acidity of titanium. Fixation of DIFP in the axial position of Fe(III) sites in MIL-100(Fe) is much less favorable, -4.82 kJ mol^{-1}, suggesting that the low performance of this material for the degradation of DIFP might be linked to an ineffective activation of the P=O bond. This value is significantly higher for MUV-101(Fe) via Fe, -11.58 kJ mol^{-1}, but still less favorable than fixation to Ti(IV), which is more likely to be dominant (Figure 6). We next looked into the hydrolysis reaction by assuming that the nucleophilic attack of the activated Ti(IV)–O=P(V) bond would involve a OH$^-$ anion generated by M(II/III/IV)–X (X = H$_2$O, OH$^-$, O^{2-}) sites in close proximity. For MUV-101(Fe), this would correspond to the transition state (TS) represented in Figure 5B (see also Figure S53). TS2 is a concerted step that involves the dissociation of a water molecule to generate nucleophilic OH$^-$ by interaction with a Fe(III)–OH site acting as a Brönsted base that will attack the P center in the DIFP molecule bond to the neighboring Ti(IV) acid site for final hydrolysis of the P–F bond. The basicity of the iron sites can be regenerated by the fluoride anions produced during the hydrolysis reaction or by proton exchanged with the solvent (See Video S1 for an overview of the degradation mechanism). Figure 5C summarizes the calculated activation energy barriers of TS2 for homometallic MIL-100(Ti) (200.7 kJ mol^{-1}), MIL-100(Fe) (70.4 kJ mol^{-1}), and heterometallic MUV-101(Co) (288.5 kJ mol^{-1}), and MUV-101(Fe) (59.8 kJ mol^{-1}) (Table S18). This confirms that DIFP hydrolysis in MUV-101(Fe) is the most favorable of all.
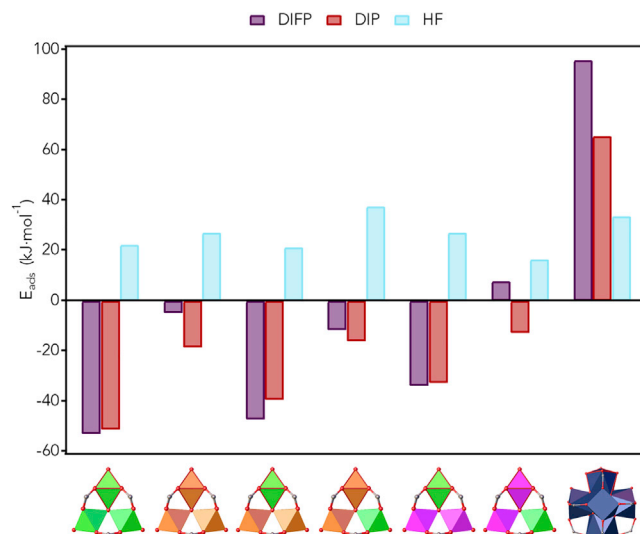
Figure 6. Adsorption Energy of Reactants and Products by Water Displacement at the Axial Positions of Ti(IV) (Green), Fe(III) (Orange), Co(II) (Magenta), or Zr(IV) (Blue) in the Homo- and Heterometallic Clusters of MIL-100(Ti), MIL-100(Fe), and MUV-101(Fe) via Ti and via Fe, MUV-101(Co) via Ti and via Co, and UiO-66(Zr)

To put these numbers into context, we also compared the activation energies calculated for this cooperative process with those reported for the accepted mechanism of Zr(IV)-MOFs (Table S19).[43] In the case of Zr(IV), the water displacement by the nerve agent is the rate determining step (RDS) with a minimum activation energy of 91.8 kJ mol^{-1} for MOF-808.[44] In our case, this process only limits the reactivity of MIL-100(Fe), whereas all MOFs containing Ti(IV) undertake water displacement quite easily, likely boosted by the acidity of this metal. In our case, the RDS is the nucleophilic attack by a dissociated water molecule, that is much more favorable for the MUV-101(Fe) from the increased strength of Fe-OH sites as a Brönsted base. Our results suggest that the inactivity of MIL-100(Ti) and MUV-101(Co), together with the poor performance reported for MIP-177,[21] originate from the absence of this basic site. Just like for PAP enzymes, the synergetic cooperation of Ti(IV) and Fe(III) centers in this dual-metal catalyst leads to a much lower energy barrier (59.8 kJ mol^{-1}) for more efficient degradation of DIFP in absence of a base.

We also used this model to evaluate the affinity of the products of the hydrolysis to bind the metal active sites, which might lead to the poisoning of the catalyst for concomitant drop of the catalytic activity. To avoid this scenario, the adsorption energy of the reactants must be greater than the adsorption energy of the products derived from partial hydrolysis of DIFP molecules. Our calculations suggest that the DIFP molecules are much strongly adsorbed than the products (DIP and HF) if the adsorption proceeds via Ti(IV) sites, which can be, in turn, desorbed more easily in the presence of water and reactant molecules (see Figure 6; Table S20). Adsorption of DIP is slightly favorable for the case of MUV-101(Fe), which might result in partial competition with the activation of DIFP. These predictions are consistent with our inhibition tests (Figure S39). Whereas the activity of MUV-101(Fe) is not altered significantly in the presence of an excess of fluoride, the addition of an equimolar amount of DIP causes a drop in the reaction rate that can be recovered back by washing the solid in water.

Effect of the Heteroatom on the Acidity of the Framework

Our computational study suggests that the differences in activity for DIFP degradation are associated to the changes in basicity of the M–X sites in the homo- and
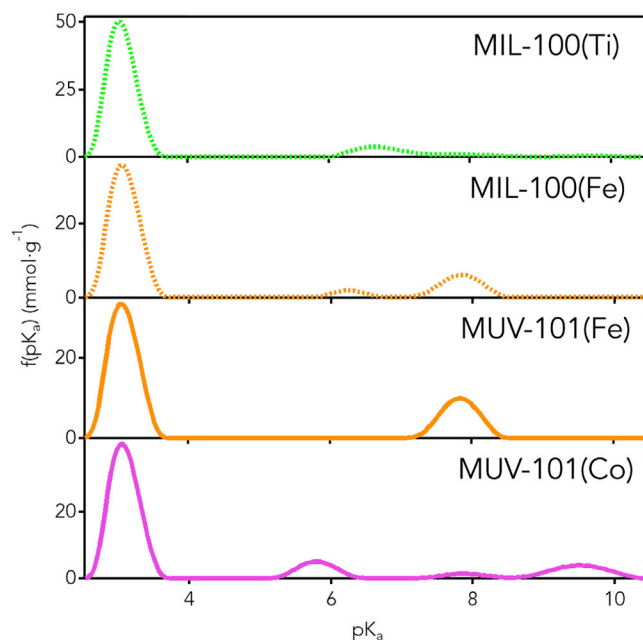
Figure 7. Effect of the Heteroatom over the Acidity of the Frameworks
Density of acid centers and pKa distribution obtained by fitting the proton binding curve extracted from the titration curves in water. From top to bottom: MIL-100(Ti), MIL100(Fe), MUV-101(Fe), and MUV-101(Co).

heterometallic clusters of the MOFs studied. This is similar to the changes in the hydrolytic activity of phosphotriesterase enzymes (PTEs) ascribed to the ability of different metals to modify the pK_a of the bounded water or hydroxide molecules.[33]

We argued that the acidity of the different MIL-100 solids would be controlled by the Lewis acidity of the different metal ions and the changes in the axially coordinated capping linkers (X = H_2O, OH^-, O^{2-}) to maintain charge balance.[45] The experimental acidity of the solids was evaluated by potentiometric acid-base titrations (See Section S7 for experimental details). The density of acid centers and pK_a distribution was determined for each MOF by fitting the proton binding curve extracted from the titration curves by using the SAEIUS numerical procedure.[46,47] The four solids showed different titration curves and changes in the distribution of acid centers for different pK_a values (Figures 7 and S55–S58). All of them show a predominant peak centered at $pK_{a0} \approx 3.1$, that can be attributed to the protonation of all the oxo, hydroxo axial groups at very low pH. Noticeable differences can be observed at higher pK_a values, that can be linked to variations in the metal and capping linkers. MIL-100(Ti) shows an almost flat pK_a distribution above 4.0, consistent with a highly acidic environment. In turn, MIL-100(Fe) and MUV-101(Fe) showed a more basic character with a more marked and narrower pK_{a1} contribution with an average pK_{a1} centered around 7.9 that we ascribe to the loss of Fe(III)–OH protons. The titration curve of MUV-101(Co) is more complex due to the presence of Co–H_2O species in the cluster. Compared to Ti(IV) and Fe(III), Co(II) is a weaker Lewis acid, but axial H_2O molecules can easily lose a proton to render Co–OH^-. This results in two contributions at pK_{a1} = 5.78 (Co–OH_2) and pK_{a2} = 9.54 (Co–OH^-). Considering pK_{a1} as the dominant acid-base equilibria for the reaction conditions (non-buffered water), the higher basicity of MUV-101(Fe) combined with more favorable adsorption of DIFP is consistent with the proposed origin for its catalytic activity.

Concluding Remarks

The combination of Ti(IV) with other transition metals can be an efficient tool to produce materials with tunable function, provided good control of the distribution of the metals across the framework. This route can combine the advantageous properties of the frameworks produced from this naturally abundant metal: excellent chemical stability, low toxicity or photoactivity, with synergetic cooperation for improved catalytic performance. We have illustrated this concept for a new family of titanium heterometallic frameworks MUV-101(Mg, Fe, Co, and Ni). Compared with other homo- and heterometallic MOFs, MUV-101(Fe) is very efficient in degrading DIFP in aqueous medium and non-buffered conditions. The activity of the pristine material does not rely on pre-conditioning with basic buffers or metal-alkoxides, thus simplifying its potential integration in protective clothing or gas masks.

We use an integrative experimental-computational approach to clarify the origin of the distinctive catalytic performance that arises from this specific combination of metals and is not accessible to the isostructural homometallic analogs. Our simulations suggest that the activity of MUV-101(Fe) is due to synergetic cooperation of Ti(IV) Lewis acid and Fe(III)–OH Brönsted base sites for a cooperative mechanism that mimics bimetallic PAP enzymes. To the best of our knowledge, this is the first example of a dual-metal TS in heterometallic MOFs that enables clear understanding of the individual roles played by the metals combined and their mutual cooperation. We are confident our results represent an excellent platform to guide the design of other heterometallic frameworks and span the increasing interest in this family of MOFs[48,49] to a broad scope of cascade or tandem reactions in which synergetic catalysis might yield unprecedented boosts in performance.

EXPERIMENTAL PROCEDURES

Resource Availability

Lead Contact

Further information and requests for resources and materials should be directed to and will be fulfilled by the Lead Contact, Carlos Martí-Gastaldo (carlos.marti@uv.es).

Materials Availability

All materials generated in this study are available from the Lead Contact with a completed Materials Transfer Agreement.

Data and Code Availability

The X-ray crystallographic data for the structure of MUV-101(Fe) reported in this paper have been deposited in the Cambridge Crystallographic Data Centre (CCDC) with the code 1960226 and can be obtained free of charge via www.ccdc.cam.ac.uk/data_request/cif.

Detailed experimental procedures are provided in the Supplemental Information.

SUPPLEMENTAL INFORMATION

Supplemental Information can be found online at https://doi.org/10.1016/j.chempr.2020.09.002.

AUTHOR CONTRIBUTIONS

C.M.-G. was responsible for the overall conception, direction, and supervision of the project. J.C.-G. and N.M.P. performed most of the experimental work and data analysis. M.R.-A. assisted with the experimental work. N.A.-B. and S.T. were responsible for the computational work. N.M.P., R.G.-S.-M., V.T., and J.A.R.N. carried out the catalytic tests. J.C.-G. and I.d.S. carried out the structural analysis. J.C.W. and B.C.J.V. carried out the Mössbauer data collection and analysis. J.J. performed the data analysis of the potentiometric titration experiments. All authors discussed the results and contributed to the writing of the manuscript.

DECLARATION OF INTERESTS

The authors declare that Universidad de València has applied for a patent on the materials discussed herein, on which J.C.-G., N.M.P., N.A.B., R.G.-S.-M., S.T., J.A.R.N., and C.M.-G. are included as inventors.

REFERENCES

1. Furukawa, H., Cordova, K.E., O'Keeffe, M., and Yaghi, O.M. (2013). The chemistry and applications of metal-organic frameworks. Science 341, 1230444.

2. Matito-Martos, I., Moghadam, P.Z., Li, A., Colombo, V., Navarro, J.A.R., Calero, S., and Fairen-Jimenez, D. (2018). Discovery of an optimal porous crystalline material for the capture of chemical warfare agents. Chem. Mater. 30, 4571–4579.

3. Mason, J.A., Oktawiec, J., Taylor, M.K., Hudson, M.R., Rodriguez, J., Bachman, J.E., Gonzalez, M.I., Cervellino, A., Guagliardi, A., Brown, C.M., et al. (2015). Methane storage in flexible metal-organic frameworks with intrinsic thermal management. Nature 527, 357–361.

4. Cadiau, A., Adil, K., Bhatt, P.M., Belmabkhout, Y., and Eddaoudi, M. (2016). A metal-organic framework-based splitter for separating propylene from propane. Science 353, 137–140.

5. Horcajada, P., Chalati, T., Serre, C., Gillet, B., Sebrie, C., Baati, T., Eubank, J.F., Heurtaux, D., Clayette, P., Kreuz, C., et al. (2010). Porous metal-organic-framework nanoscale carriers as a potential platform for drug delivery and imaging. Nat. Mater. 9, 172–178.

6. Mondloch, J.E., Katz, M.J., Isley, W.C., Ghosh, P., Liao, P., Bury, W., Wagner, G.W., Hall, M.G., Decoste, J.B., Peterson, G.W., et al. (2015). Destruction of chemical warfare agents using metal-organic frameworks. Nat. Mater. 14, 512–516.

7. Zhao, M., Yuan, K., Wang, Y., Li, G., Guo, J., Gu, L., Hu, W., Zhao, H., and Tang, Z. (2016). Metal-organic frameworks as selectivity regulators for hydrogenation reactions. Nature 539, 76–80.

8. Liu, Y., Howarth, A.J., Vermeulen, N.A., Moon, S.Y., Hupp, J.T., and Farha, O.K. (2017). Catalytic degradation of chemical warfare agents and their simulants by metal-organic frameworks. Coord. Chem. Rev. 346, 101–111.

9. Bobbitt, N.S., Mendonca, M.L., Howarth, A.J., Islamoglu, T., Hupp, J.T., Farha, O.K., and Snurr, R.Q. (2017). Metal-organic frameworks for the removal of toxic industrial chemicals and chemical warfare agents. Chem. Soc. Rev. 46, 3357–3385.

10. Barea, E., Maldonado, C.R., and Navarro, J.A.R. (2018). MOFs for the capture and degradation of chemical warfare agents. In Metal-Organic Frameworks: Applications in Separations and Catalysis, H. García and S. Navalón, eds. (Wiley-VCH Verlag), pp. 199–221.

11. López-Maya, E., Montoro, C., Rodríguez-Albelo, L.M., Aznar Cervantes, S.D., Lozano-Pérez, A.A., Cenís, J.L., et al. (2015). Textile/metal-organic-framework composites as self-detoxifying filters for chemical-warfare agents. Angew. Chem. Int. Ed. 54, 6790–6794.

12. Moon, S.Y., Liu, Y., Hupp, J.T., and Farha, O.K. (2015). Instantaneous hydrolysis of nerve-agent simulants with a six-connected zirconium-based metal-organic framework. Angew. Chem. Int. Ed. 54, 6795–6799.

13. Plonka, A.M., Wang, Q., Gordon, W.O., Balboa, A., Troya, D., Guo, W., Sharp, C.H., Senanayake, S.D., Morris, J.R., Hill, C.L., and Frenkel, A.I. (2017). In situ probes of capture and decomposition of chemical warfare agent simulants by Zr-based metal organic frameworks. J. Am. Chem. Soc. 139, 599–602.

14. Chen, Z., Wang, X., Noh, H., Ayoub, G., Peterson, G.W., Buru, C.T., et al. (2019). Scalable, room temperature, and water-based synthesis of functionalized zirconium-based metal-organic frameworks for toxic chemical removal. Cryst. Eng. Comm. 21, 2409–2415.

15. Katz, M.J., Moon, S.Y., Mondloch, J.E., Beyzavi, M.H., Stephenson, C.J., Hupp, J.T., and Farha, O.K. (2015). Exploiting parameter space in MOFs: A 20-fold enhancement of phosphate-

ester hydrolysis with UiO-66-NH2. Chem. Sci. 6, 2286–2291.

16. Gil-San-Millan, R., López-Maya, E., Hall, M., M. Padial, N., Peterson, G.W., DeCoste, J.B., et al. (2017). Chemical warfare agents detoxification properties of zirconium metal-organic frameworks by synergistic incorporation of nucleophilic and basic sites. ACS Appl. Mater. Interfaces 9, 23967–23973.

17. De Koning, M.C., Van Grol, M., and Breijaert, T. (2017). Degradation of paraoxon and the chemical warfare agents VX, tabun, and Soman by the metal-organic frameworks UiO-66-NH2, MOF-808, NU-1000, and PCN-777. Inorg. Chem. 56, 11804–11809.

18. Kalaj, M., Palomba, J.M., Bentz, K.C., and Cohen, S.M. (2019). Multiple functional groups in UiO-66 improve chemical warfare agent simulant degradation. Chem. Commun. 55, 5367–5370.

19. Gil-San-Millan, R., López-Maya, E., Platero-Prats, A.E., Torres-Pérez, V., Delgado, P., Augustyniak, A.W., Kim, M.K., Lee, H.W., Ryu, S.G., and Navarro, J.A.R. (2019). Magnesium exchanged zirconium metal–organic frameworks with improved detoxification properties of nerve agents. J. Am. Chem. Soc. 141, 11801–11805.

20. M. Padial, N., Castells-Gil, J., Almora-Barrios, N., Romero-Angel, M., Da Silva, I., Barawi, M., et al. (2019). Hydroxamate titanium-organic frameworks and the effect of siderophore-type linkers over their photocatalytic activity. J. Am. Chem. Soc. 141, 13124–13133.

21. Vieira Soares, C., Maurin, G., and Leitão, A.A. (2019). Computational exploration of the catalytic degradation of Sarin and its simulants by a titanium metal–organic framework. J. Phys. Chem. C 123, 19077–19086.

22. Assi, H., Mouchaham, G., Steunou, N., Devic, T., and Serre, C. (2017). Titanium coordination compounds: from discrete metal complexes to metal-organic frameworks. Chem. Soc. Rev. 46, 3431–3452.

23. Castells-Gil, J., M. Padial, N., Almora-Barrios, N., Da Silva, I., Mateo, D., Albero, J., et al. (2019). De novo synthesis of mesoporous photoactive titanium(iv)-organic frameworks with MIL-100 topology. Chem. Sci. 10, 4313–4321.

24. Férey, G., Serre, C., Mellot-Draznieks, C., Millange, F., Surblé, S., Dutour, J., et al. (2004). A hybrid solid with giant pores prepared by a combination of targeted chemistry, simulation, and powder diffraction. Angew. Chem. Int. Ed. 43, 6296–6301.

25. Bueken, B., Vermoortele, F., Vanpoucke, D.E.P., Reinsch, H., Tsou, C.C., Valvekens, P., et al. (2015). A flexible photoactive titanium metal-organic framework based on a [TiIV3(μ3-O)(O)2(COO)6] cluster. Angew. Chem. Int. Ed. 54, 13912–13917.

26. Mason, J.A., Darago, L.E., Lukens, W.W., and Long, J.R. (2015). Synthesis and O2 reactivity of a titanium(III) metal-organic framework. Inorg. Chem. 54, 10096–10104.

27. Wongsakulphasatch, S., Nouar, F., Rodriguez, J., Scott, L., Le Guillouzer, C., Devic, T., et al. (2015). Direct accessibility of mixed-metal (iii/ii) acid sites through the rational synthesis of porous metal carboxylates. Chem. Commun. 51, 10194–10197.

28. Zhai, Q.G., Bu, X., Mao, C., Zhao, X., Daemen, L., Cheng, Y., Ramirez-Cuesta, A.J., and Feng, P. (2016). An ultra-tunable platform for molecular engineering of high-performance crystalline porous materials. Nat. Commun. 7, 13645.

29. Wang, Y., Zhao, X., Yang, H., Bu, X., Wang, Y., Jia, X., et al. (2019). A tale of two trimers from two different worlds: a COF-inspired synthetic strategy for pore-space partitioning of MOFs. Angew. Chem. Int. Ed. 58, 6316–6320.

30. Giménez-Marqués, M., Santiago-Portillo, A., Navalón, S., Álvaro, M., Briois, V., Nouar, F., Garcia, H., and Serre, C. (2019). Exploring the catalytic performance of a series of bimetallic MIL-100(Fe, Ni) MOFs. J. Mater. Chem. A 7, 20285–20292.

31. Yang, H., Wang, Y.Y., Krishna, R., Jia, X., Wang, Y.Y., Hong, A.N., Dang, C., Castillo, H.E., Bu, X., and Feng, P. (2020). Pore-space-partition-enabled exceptional ethane uptake and ethane-selective ethane-ethylene separation. J. Am. Chem. Soc. 142, 2222–2227.

32. Castells-Gil, J., M. Padial, N., Almora-Barrios, N., Albero, J., Ruiz-Salvador, A.R., González-Platas, J., et al. (2018). Chemical engineering of photoactivity in heterometallic titanium–organic frameworks by metal doping. Angew. Chem. Int. Ed. 57, 8453–8457.

33. Kimura, E. (2000). Dimetallic hydrolases and their models. Curr. Opin. Chem. Biol. 4, 207–213.

34. Zou, L., Feng, D., Liu, T.F., Chen, Y.P., Yuan, S., Wang, K., Wang, X., Fordham, S., and Zhou, H.C. (2016). A versatile synthetic route for the preparation of titanium metal-organic frameworks. Chem. Sci. 7, 1063–1069.

35. M. Padial, N., Lerma-Berlanga, B., Almora-Barrios, N., Castells-Gil, J., Da Silva, I., De La Mata, M., et al. (2020). Heterometallic titanium-organic frameworks by metal-induced dynamic topological transformations. J. Am. Chem. Soc. 142, 6638–6648.

36. Llewellyn, P.L., Bourrelly, S., Serre, C., Vimont, A., Daturi, M., Hamon, L., De Weireld, G., Chang, J.S., Hong, D.Y., Kyu Hwang, Y.K., et al. (2008). High uptakes of CO2 and CH4 in mesoporous metal-organic frameworks MIL-100 and MIL-101. Langmuir 24, 7245–7250.

37. Jiao, Y., Morelock, C.R., Burtch, N.C., Mounfield, W.P., Hungerford, J.T., and Walton, K.S. (2015). Tuning the kinetic water stability and adsorption interactions of Mg-MOF-74 by partial substitution with co or Ni. Ind. Eng. Chem. Res. 54, 12408–12414.

38. Hall, J.N., and Bollini, P. (2020). Quantification of open-metal sites in metal-organic frameworks using irreversible water adsorption. Langmuir 36, 1345–1356.

39. Rubio-Giménez, V., Waerenborgh, J.C., Clemente-Juan, J.M., and Martí-Gastaldo, C. (2017). Spontaneous magnetization in heterometallic NiFe-MOF-74 microporous magnets by controlled iron doping. Chem. Mater. 29, 6181–6185.

40. Jang, Y.J., Kim, K., Tsay, O.G., Atwood, D.A., and Churchill, D.G. (2015). Update 1 of: destruction and detection of chemical warfare agents. Chem. Rev. 115, PR1–PR76.

41. Katz, M.J., Mondloch, J.E., Totten, R.K., Park, J.K., Nguyen, S.T., Farha, O.K., et al. (2014). Simple and compelling biomimetic metal-organic framework catalyst for the degradation of nerve agent simulants. Angew. Chem. Int. Ed. 53, 497–501.

42. Erxleben, A. (2019). Mechanistic studies of homo- and heterodinuclear zinc phosphoesterase mimics: what has been learned? Front. Chem. 7, 82.

43. Momeni, M.R., and Cramer, C.J. (2019). Computational screening of roles of defects and metal substitution on reactivity of different single- vs double-node metal-organic frameworks for Sarin decomposition. J. Phys. Chem. C 123, 15157–15165.

44. Rosen, A.S., Notestein, J.M., and Snurr, R.Q. (2019). Identifying promising metal–organic frameworks for heterogeneous catalysis via high-throughput periodic density functional theory. J. Comput. Chem. 40, 1305–1318.

45. Klet, R.C., Liu, Y., Wang, T.C., Hupp, J.T., and Farha, O.K. (2016). Evaluation of Brønsted acidity and proton topology in Zr- and Hf-based metal-organic frameworks using potentiometric acid-base titration. J. Mater. Chem. A 4, 1479–1485.

46. Jagiełło, J. (1994). Stable numerical solution of the adsorption integral equation using splines. Langmuir 10, 2778–2785.

47. Jagiełło, J., Bandosz, T.J., Putyera, K., and Schwarz, J.A. (1995). Determination of proton affinity distributions for chemical systems in aqueous environments using a stable numerical solution of the adsorption integral equation. J. Colloid Interface Sci. 172, 341–346.

48. Abednatanzi, S., Gohari Derakhshandeh, P., Depauw, H., Coudert, F.X., Vrielinck, H., Van Der Voort, P., and Leus, K. (2019). Mixed-metal metal-organic frameworks. Chem. Soc. Rev. 48, 2535–2565.

49. Masoomi, M.Y., Morsali, A., Dhakshinamoorthy, A., and Garcia, H. (2019). Mixed-metal MOFs: unique opportunities in metal–organic framework (MOF) functionality and design. Angew. Chem. Int. Ed. 58, 15188–15205.